PUBLICATIONS OF THE ASTRONOMICAL SOCIETY OF THE PACIFIC, **124**:861–867, 2012 August

A Highly Efficient Lucky Imaging Algorithm: Image Synthesis Based on Fourier Amplitude Selection

VINCENT GARREL,[1] OLIVIER GUYON,[1] AND PIERRE BAUDOZ[2]

Received 2011 May 27; accepted 2012 June 14; published 2012 August 30

ABSTRACT. We propose a new algorithm dramatically enhancing the efficiency of the lucky imaging technique for AO-corrected images in the visible range. It is achieved by a selection based on the relative strength of signal for each spatial frequency in the Fourier domain, making a more efficient use of information contained in each frame. Realistic simulations show that our algorithm allows us to reach the diffraction limit in the visible range on an AO-equipped 8 m telescope and enhances the Strehl ratio of an AO long exposure by a factor of up to 4. It outperforms the lucky imaging technique at an equivalent selection ratio. The fraction of selected data in simulation is also boosted from two to eight times for a given Strehl-ratio performance.

1. INTRODUCTION

Atmospheric turbulence dynamically distorts the plane wave front originating from astronomical objects, generating a rapidly changing interference pattern in the image plane, known as speckles. In a long-exposure frame, these speckles quickly average, and the resulting point-spread function (PSF) is then limited at the arcsecond scale. This severely degrades the theoretical angular resolution of a large telescope, which is in the tens of milliarcseconds scale in the visible range. Under the coherence time of the atmosphere, i.e., milliseconds to tens of milliseconds, the distorted phase can be approximated as "frozen." Short-exposure frames in the image plane record unblurred speckles that still retain high-resolution information, up to the diffraction limit of the telescope. Starting with the pioneering work of Labeyrie (1970), a number of techniques have been proposed to take advantage of short-exposure frames in order to recover the loss of resolution. They can be can divided into real-time correction techniques and postprocessing techniques. In the real-time techniques, a fast analysis of the instantaneous wave front is performed to drive a mirror allowing a partial correction of the distortion. We can cite the very successful adaptive-optics (AO) systems (Babcock 1953; Hardy et al. 1977; Rousset et al. 1990), but we also note the speckle stabilization technique (Keremedjiev & Eikenberry 2011). Postprocessing techniques, under the generic name of speckle imaging, use a set of recorded short-exposure frames and knowledge about statistics of the turbulence to recover diffraction-limited images from the original object (Knox & Thompson 1974; Weigelt 1977; Beckers 1983; Paxman & Seldin 1993).

Lucky imaging is probably the simplest of these postprocessing techniques. It was first designed to take advantage of the wide statistical distribution of atmospheric turbulent wave fronts and selects only the least aberrated short-exposure frames, close to the diffraction limit. Different criteria have been proposed to select these frames (Roggemann & Welsh 1995), such as the sharpness of the image criteria (Muller & Buffington 1974), but the most widely used remains the instantaneous Strehl ratio. The probability of getting a short-exposure image of good quality, i.e., the wave front distortion over the pupil is 1 rad rms or less, has previously been described for atmospheric turbulence (Fried 1978). The probability depends on the ratio between the diameter of the telescope and the Fried parameter r_o, which is the coherence length of the distorted wave front (Fried 1966). Lucky imaging recently gained some new interest with the availability of electron multiplying charge-coupled device (EMCCD) technology for visible science (Mackay et al. 2004; Law et al. 2006; Hormuth et al. 2007; Rodríguez Ramos et al. 2008; Labadie et al. 2010). It offers extremely low readout noise (and an excess photon noise factor of 1.4), allowing the summing of short-exposure images without loss of the overall signal-to-noise ratio.

The advantages of the lucky imaging technique over the long-exposure case are twofold: (1) the frame selection process rejects the worst aberrated frames, improving the resolution of the final image issued from a stack of the selected short-exposure frames, and (2) short-exposure images are recentered before being added together. This process of recentering in the focal plane, described as "shift-and-add," is equivalent to a tip-tilt correction of the wave front in the pupil plane running at the frequency of frame acquisition (if images are taken continuously). So, even without the selection process, the resultant image issued from stacking short-exposure frames still offers an improved resolution over its long-exposure counterpart (Fried 1966).

[1] Subaru Telescope, 650 N. A'Ohoku Place., Hilo, HI.
[2] Laboratoire d'tudes spatiales et d'instrumentation en astrophysique, Observatoire de Paris-Meudon, 5 place Jules Janssen, F-92195, Meudon, France.

Due to the generalization of AO-systems on large telescopes, the size of the equivalent of r_o at the output of an AO system (Cagigal & Canales 1998) and the distribution of the instantaneous Strehl ratio among AO-corrected short-exposure images have also been investigated for different AO-correction regimes (Fusco & Conan 2004; Gladysz et al. 2006; Gladysz et al. 2008). A combination of lucky imaging with an AO system on a large telescope has been already realized by Law et al. (2009), demonstrating promising results. For the Subaru coronagraphic extreme AO (SCExAO) visible science path, we propose here a hybrid algorithm of lucky imaging and speckle interferometry, demonstrating improved results over classic lucky imaging.

In § 2, we introduce the principles behind the chosen criterion we propose in this article. The implementation of the algorithm follows in § 3. Comparative performances of this algorithm with a classic lucky imaging algorithm based on a set of simulated images are discussed in § 4. Discussion and the conclusion are given in § 5.

2. PRINCIPLE

2.1. Lucky Imaging: State of the Art and Limits

In the case of a hybrid AO and lucky imaging system, the gain in resolution obtained by the lucky imaging technique is a steep function of the selection ratio. Compared with the equivalent long exposure of a single star with adaptive optics at the Palomar Hale Telescope, which tops at 6% Strehl ratio at 710 nm, Law et al. (2009) obtained a gain of two in Strehl ratio with a 10% selection fraction (and an even higher gain of three in the case of a 1% selection) issued from a set of short exposures at 50 frames s^{-1} with a narrowband filter. The gain in FWHM for the same selection is 2, which gives images very close to the diffraction limit at 35 mas for a 5 m telescope.

The high gain at the 1% selection fraction is, however, not used for science purposes as it leads to a quite poor photometric sensitivity. A method increasing this photometric sensitivity while keeping the same angular resolution performance is important in order to mitigate this current trade-off between image quality and observation time. For this purpose, we need to refine the selection process and seek valuable information previously overlooked. To our knowledge, previously proposed algorithms and their associated criteria always consider the whole short-exposure frame as a basic unit to select or discard. While intuitive and easy to implement, this approach suffers two drawbacks: the first is to partially or totally reject short-exposure frames presenting good resolution only in a given direction. The second is linked to the choice of a criterion itself: it will favor the selection of fine details over the general shape, or the inverse. In the case of the widely used instantaneous Strehl ratio, the criterion selects images presenting the best concentration of energy in the central speckle, i.e., minimal low spatial frequency aberrations, which is equivalent to a good resolution of general shapes; if some frames contain fine details relatively untainted by aberrations, i.e., in high spatial frequencies but with a strong low-frequency aberration, this valuable information will be discarded.

2.2. Image Formation

The Fourier transform of an image is a suitable view to describe how each spatial frequency is modified by atmospheric turbulence. Each short-exposure frame i_n is formed by the convolution of the constant object $o(x, y)$ by a variable point-spread function PSF_n:

$$i_n(x, y) = o(x, y) * \mathrm{PSF}_n(x, y). \tag{1}$$

By applying the Fourier transform, the optical transfer function (OTF) of the full optical system appears as follows:

$$I_n(u, v) = O(u, v).\mathrm{OTF}_n(u, v). \tag{2}$$

The OTF can be decomposed into the $\mathrm{OTF}_{\mathrm{DL}}$, the diffraction-limited low-pass filter representing the static transfer function of the telescope alone, and a dynamic OTF_n of the atmosphere distorted by turbulence:

$$\mathrm{OTF}_n(u, v) = \mathrm{OTF}_{\mathrm{DL}}(u, v).\mathrm{OTF}_{n\,\mathrm{atmo}}(u, v). \tag{3}$$

A Fourier transform of the perfect diffraction-limited image is given by the multiplication of the object $O(u, v)$ with the $\mathrm{OTF}_{\mathrm{DL}}$ of the telescope only. Equation (3) becomes

$$I_n(u, v) = I_{\mathrm{DL}}(u, v).\mathrm{OTF}_{n\,\mathrm{atmo}}(u, v), \tag{4}$$

where I_{DL} is the theoretical telescope diffraction-limited image. The amplitude of the OTF is also called the modulation transfer function (MTF):

$$|I_n(u, v)| = |I_{\mathrm{DL}}(u, v)|.\mathrm{MTF}_{n\,\mathrm{atmo}}(u, v). \tag{5}$$

The $\mathrm{MTF}_{n\,\mathrm{atmo}}(u, v)$ is a factor representing the attenuation of Fourier amplitude due to abberations introduced by atmospheric turbulences, and as such is always less than unity (Goodman 1996):

$$\mathrm{MTF}_{n\,\mathrm{atmo}}(u, v) = \frac{|I_n(u, v)|}{|I_{\mathrm{DL}}(u, v)|} \leq 1. \tag{6}$$

Selecting the fraction of data with the highest signal in $|I_n(u, v)|$ corresponds to a minimization of the $\mathrm{MTF}_{n\,\mathrm{atmo}}$, i.e., it reduces the power of atmospheric abberations on the final image that cause the blur of r_o/D-size in a long-exposure image. Since there is no constraint added on the phase of $I_n(u, v)$ which encodes the spatial position of objects in frames, this method works on any object bright enough to allow frames to be recentered accurately and does not require any calibration on a reference star. This MTF ratio is very similar to the Strehl

ratio but applies to each spatial frequency separately, providing a finer way to select information.

2.3. Image Synthesis Principle Based on One Example

In Figure 1, we show a typical image issued from a simulation representing a short-exposure frame of a partially corrected PSF at 650 nm without photon noise. This image has been centered on its brightest pixel. The correction is achieved by the Subaru AO188 system designed for near-IR (see § 4 for a more detailed description of the simulation). Its Fourier transform amplitude is represented in the right image. All the spatial information is contained in a disk: since the PSF is the Fourier transform of the complex amplitude of the signal in a circular pupil plane, the low spatial frequencies response is located in the center of the image, whereas the high frequencies response stands close to the perimeter of the circle. As described in equation (6), the amplitude is attenuated compared with the diffraction limit MTF, but with very different levels of signal (in white and light gray) in the focal plane as phase aberrations arise in the pupil plane due to the turbulent atmosphere. However, the short-exposure frame keeps a relatively good signal for some high frequencies, and this is represented by the short-exposure MTF radial profile being higher or equal to the long-exposure MTF radial profile angle.

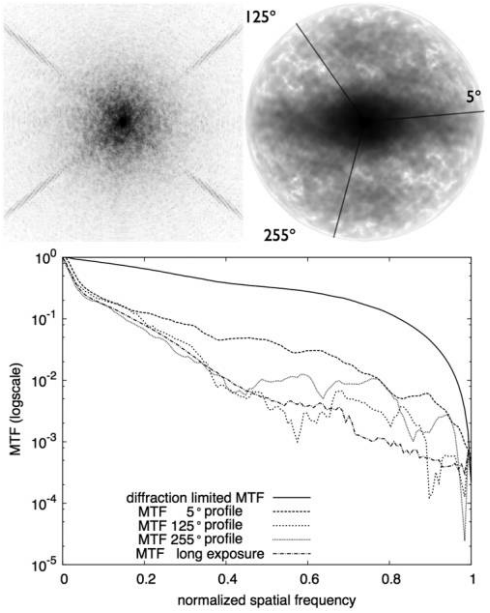

FIG. 1.—Typical PSF image (*top left*) and its corresponding MTF image (*top right*) of a simulated short-exposure frame of a star, as achieved by the Subaru Telescope at 650 nm, after correction of the AO188 adaptive-optics system. Speckles in the image plane translate to attenuation of the perfect, diffraction-limited MTF signal. From the MTF signal, three radial profiles issued from the bias frequency at a given angle have been extracted and compared (*lower*) to a diffraction-limited profile and a long-exposure MTF made from a 4 min long exposure simulated with the same atmospheric conditions.

As an example of the spatial variability of MTF_{atmo}, we show three radial profiles along three position angles extracted from this example amplitude . In the 5° radial profile, the Fourier transform amplitude contains the attenuated signal, about 1 order of magnitude lower than the diffraction-limited MTF for the mid-frequency regime, i.e., from 0.2 to 0.8 of the frequency cut-off. In the 255° radial profile,the Fourier transform amplitude contains a very attenuated signal all along its profile, meaning that the phase aberrations of turbulent atmosphere had a strong influence. It is on average 2 orders of magnitude lower than the diffraction-limited signal in the same mid-frequency regime. The 125° radial profile angle presents a very variable attenuation, as strongly attenuated as the 255° radial profile at the 0.4 cut-off frequency but as slightly attenuated as the 5° radial profile angle at a 0.75 cut-off frequency.

In this example, selecting information in the 5° radial profile and parts of the 125° radial profile at 0.75 cut-off frequency, which are only slightly attenuated compared to the diffraction-limited signal, would bring a better estimate of the ideal amplitude of the PSF. Due to the observed large statistical distribution of speckles between each frame, each image has a different pattern of attenuation for its MTF. We propose to combine selections from different images in order to cover the MTF space with an only slightly attenuated signal.

In Figure 2, we illustrate the principle of the image synthesis based on the Fourier amplitude selection technique on a simple example, using four PSFs elongated in different directions in the first row. In the second row, the amplitude of the Fourier transform of these images is shown. The third row shows selections of the region where the signal of the given frame is the strongest among the set of frames. Adding these selections together, the frequency disk is nicely covered with a strong signal. Using the complex amplitude associated with this selected amplitude, an inverse Fourier transform gives an image where aberrations are reduced and the resolution improved.

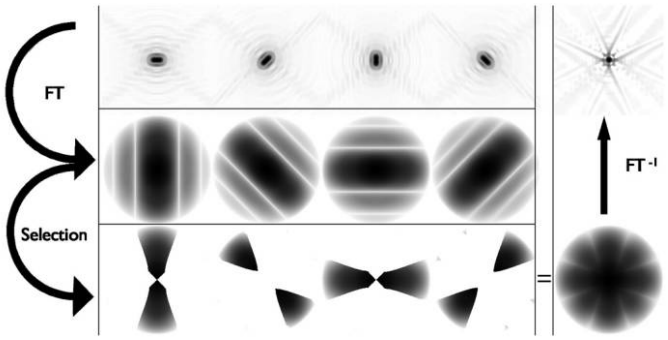

FIG. 2.—Principle of image synthesis with data from different frames. *Top:* Four PSFs abberated in different directions, the narrow axis is diffraction limited. *Middle:* Amplitude of their Fourier transform. *Bottom:* Selected information based on the maximization of amplitude. The selected values are coadded in the Fourier plane. The complex amplitude associated with the selection is used for an inverse Fourier transform. The final image displays a better resolution, closer to an unberrated PSF.

3. DATA PROCESSING OF ISFAS ALGORITHM

We present our first implementation of the image synthesis based on the Fourier amplitude selection algorithm (ISFAS) in Figure 3. We chose to regroup different operations into three different main operations according to their goal: individual preprocessing of frames, selection of information, and finally synthesis based on the selection. These main operations can be used to describe any algorithm based on the lucky imaging principle of information selection into a set of frames. In the classic lucky imaging scheme, i.e., select, shift, and add, the preprocessing consists of the shift of individual frames. The selection of information is done by selecting frames according to a criterion estimating its quality. The synthesis of selected information is simply achieved by adding up the selected frames. In the next three sections, we describe more precisely each step we used.

3.1. Individual Frame Preprocessing

Whereas the Fourier transform amplitude of the image is insensitive to the position of the object in the set of frames, the Fourier transform phase is sensitive. In order to recover as much as possible the original object phase, we need to recenter each frame. Centering on the brightest speckle has proven to yield better results than pure centroiding (Christou 1991). Subpixel accuracy for the tracking can be obtained by centroiding iteratively a clipped image around the brightest pixel (Gladysz et al. 2006). In this article, we achieve the subpixel accuracy by computing an interpolated image of the brightest speckle using a Fourier zoom through the zero-padding technique and track the brightest point of the speckle. A zoom by a factor of four provides a sufficient accuracy on the centering. In the case of a poor Strehl ratio for some frames, several speckles can present almost the same brightness. To minimize recentering errors, we decided to select the brightest speckle closest to the photocenter of the frame. From this datacube of recentered frames, we use a fast Fourier transform algorithm to compute the Fourier transform of each frame of the set. The complex values are stored in memory as they will serve as a basis for further steps.

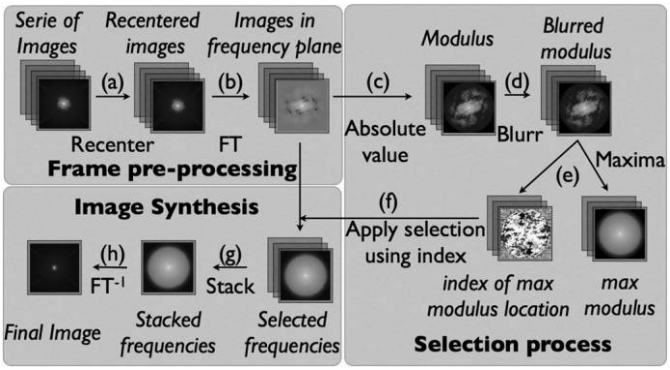

FIG. 3.—Algorithm diagram. Intermediate states of data are written in italics, operations applied to data are described in plain. Operations (*a*) to (*d*) are applied to each image in the set, then the selection reduces their number in operations (*e*) and (*f*). A final image is obtained in operations (*g*) and (*h*). For text clarity and to compare with a classic lucky imaging algorithm, operations have been grouped into three different groups: Frame preprocessing, Selection process, and Image Synthesis.

3.2. Selection Process

Our selection process consists of selecting the highest values of the Fourier transform amplitude in a set of frames for every spatial frequency in the disk inside the frequency cut-off, pixel by pixel. Like the lucky imaging algorithm, the selection ratio is a parameter requiring a trade-off between the desired sensitivity and resolution performance for given conditions such as available total time exposure and atmospheric conditions.

To achieve this selection, the first step consists in extracting the Fourier amplitude $I_n(u, v)$ from the complex datacube computed in § 3.1. The selection process chooses which complex values to keep for every spatial frequency according to their Fourier amplitude and the chosen selection fraction (see the previous section for reference). We achieve this by recording, inside an index, positions of high Fourier transform amplitude inside the datacube. This index of positions can then address the complex value datacube we kept in the previous step.

(Note: This algorithm can require a large amount of memory if every complex datacube from a long series of frames has to be stored. It can also be used in a sequential way, with only the maxima of amplitude and the index of their positions stored into RAM buffers. The set of frames stored in the preprocessing step can be then divided into several subsets.)

An additional step in the selection process is necessary to avoid, as much as possible, misselections due to the photon noise. Due to the short exposure time necessary to freeze the atmospheric turbulence, the photon noise is a significant additional source of randomness. In this case, the rate function of the Poisson process is itself a random variable, depending on the effects of the atmospheric turbulence at a given time. Such random Poisson processes are described as doubly stochastic random Poisson processes (Roggemann & Welsh 1995). The mean and variance of the combined noise can be estimated, but the relative importance of the two noises for each frame is difficult to determine.

Qualitatively, the photon noise distribution in the Fourier plane is only dependent on the total number of photons in the frame and the number of pixels receiving light, while the distribution of atmospheric turbulence noise depends from the mean attenuation of the MTF. In the high spatial frequency domain, this difference often leads the photon noise distribution level to be larger than the attenuation of the MTF due to atmospheric noise, which will corrupt our selection process.

In order to reduce the impact of photon noise distribution while maintaining the distribution of MTF attenuation, we take advantage of the different spatial correlations of the noise in the Fourier plane. The observed attenuation of MTF is very

TABLE 1
SIMULATIONS PARAMETERS

Turbulence parameters	
Spectrum model	Kolmogorov
Turbulence layers	8
Seeing	0.6″
Sampling frequency	2 kHz
Telescope and AO correction parameters	
Effective size of telescope	7.92 m
Central obstruction	2.20 m
WFS type	Curvature
Number of elements	188
Sampling frequency	1 kHz
Star brightness	$m_V = 12$
Wave front error rms	250 nm
Strehl ratio in H band	38%
Lucky imaging parameters	
Wavelength	650 nm
Spectral bandwidth	10 nm
Sampling frequency	35 Hz
Number of frames	9000

spatially correlated in the Fourier plane for small differences of spatial frequencies, while the photon noise is almost uncorrelated. Therefore, we convolve the observed Fourier transform amplitude with a small spatial Gaussian kernel to effectively average the large distribution of photon noise and keep the large distribution of MTF attenuation relatively unaffected. This smoothing affects only the selection process, as the index of selected data will address the original noisy data.

3.3. Image Synthesis

We select the Fourier complex values, including amplitude and phase, with the index provided by the previous selection process. Their relative positions in the time axis of the datacube can be disregarded, as they will be summed. Each spatial frequency in the complex plane is summed separately. From the complex values obtained, we use the fast inverse Fourier transform to return in the real image plane.

4. COMPARISON OF DIFFERENCES IN PERFORMANCE BETWEEN CLASSIC LUCKY IMAGING AND ISFAS

In this section, we introduce results from our algorithm, compared with a more classic lucky imaging based on the select, shift and add scheme, and also based on the criterion of the instantaneous Strehl ratio. The comparison is based on a common set of simulated short-exposure frames, with an end-to-end AO performance simulator designed for the 8 m Subaru Telescope (Guyon et al. 2004).[3] Parameters for the simulation have been summarized in Table 1. The input for the AO system is phase screens from a turbulent atmosphere modeled by eight thin layers at different altitudes, with different wind speeds. The output of the simulator is AO-corrected phase screens at a desired wavelength, sampled at 2 kHz. The wave front error for this simulation is 250 nm rms, corresponding to a 38% Strehl ratio in the H band.

The parameters we use for this particular simulation are a guide star of twelfth magnitude positioned at the zenith and a seeing of 0.6″, typical at the Mauna Kea summit. The output phase screens are then converted into a Nyquist-sampled

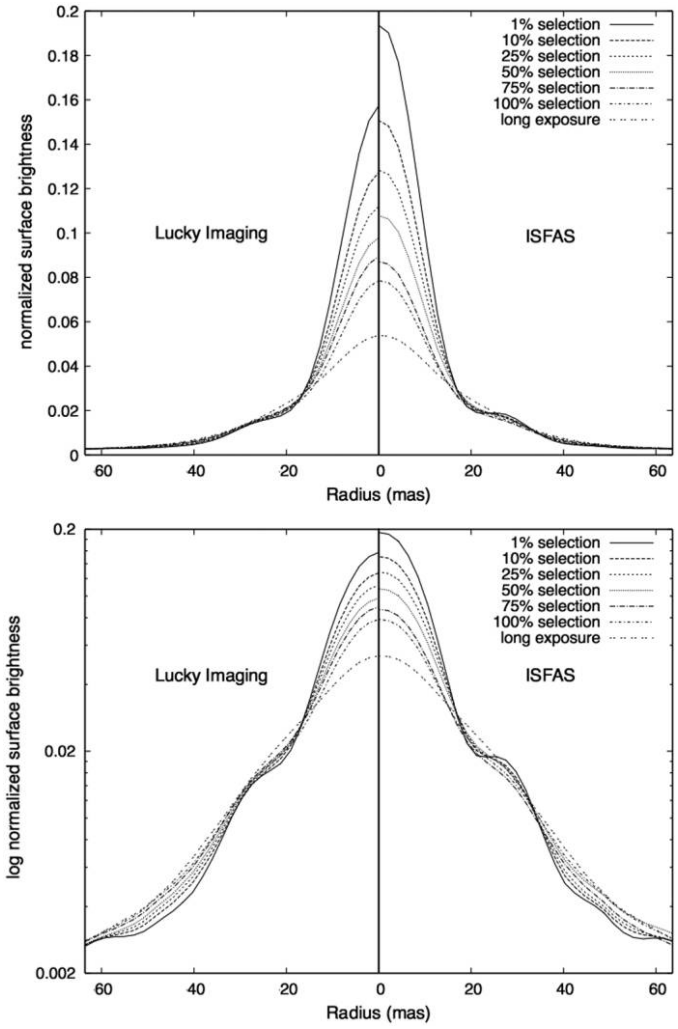

FIG. 4.—PSF radial profile as a function of data selection ratio for lucky imaging and ISFAS algorithms. Surface brightness has been normalized to diffraction-limit PSF. The surface brightness at 0 mas is by definition the Strehl ratio. The original dataset is made of 9000 simulated images sampled at 35 Hz. The chosen parameters are twelfth magnitude at zenith and 0.6″ seeing. The long-exposure case is the sum of all simulated frames without any recentering. The 100% selection case is the result of co-adding all the frames after recentering each of them. *Top:* Performances of both algorithms in linear scale. *Bottom:* The same performances are displayed in logscale. For both algorithms, the selection process increases resolution performances over AO188 alone. ISFAS allows the recovery of the second Airy ring in the case of a 1% selection.

[3] Cfits available at www.naoj.org/staff/guyon/.

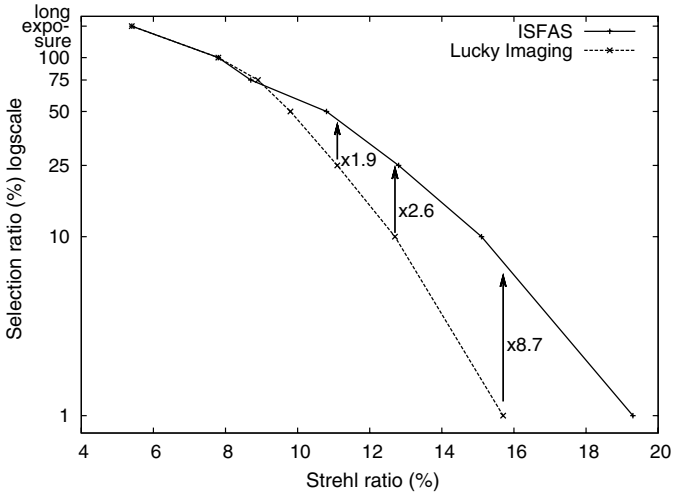

FIG. 5.—Data selection necessary to a given Strehl ratio performance for lucky imaging and Fourier synthesis algorithms. The dataset is the same set of data as Fig. 4. ISFAS algorithm performance allows the increase of the selection ratio compared with a classic lucky imaging algorithm. Logscale on the selection ratio axis has been chosen to emphasize the importance of sensitivity gain between low percentages of selection.

monochromatic PSF at 650 nm. These PSFs are then coadded together, so that the sampling drops from 2 kHz to 35 Hz, which is the actual temporal sampling of the Andor 512 by 512 EMCCD camera we use for the SCExAO visible path (Garrel et al. 2010). The final set is made of 9000 images, representing around 4 minutes, 20 seconds of exposure. This instrument on sky has a field of view of less than 5″, so we decide to not take anisoplanetism into account. To compare the performances of algorithms with pure atmospheric noise, we also did not include photon noise and assumed perfect optics. Prior to both algorithms, images have been recentered on their brightest pixel as explained in § 3.1.

Figure 4 presents radial profile obtained according to different ratios of selection for both lucky imaging and ISFAS algorithms. The Strehl ratio is measured on the guide star itself. Performances are identical for 100% selection, since it corresponds to the recentering and co-adding of all frames without any selection. ISFAS outperforms the classic lucky imaging algorithm at an equal selection rate. The ratio of energy between core and halo is also improved compared with the lucky imaging algorithm, also slightly increasing the contrast performance especially needed for faint target detection close to the central star. At the 1% selection ratio for ISFAS, the algorithm brings up a perfectly visible first Airy ring and even a faint second ring of the PSF, illustrating the high quality of the reconstruction.

Figure 5 presents an overview of the Strehl ratio obtained with both algorithms according to different ratios of selection. The most interesting performance lies in the comparison of both algorithms for a given Strehl ratio. For the same 15.7% Strehl ratio, classic lucky imaging selects no more than 1% of the best frames, whereas ISFAS can select 8.7% of the information contained in all the frames, increasing the sensitivity obtained in the final image. It also means, for the same performances in resolution and SNR, ISFAS needs 8.7 times less telescope time if the sample of images is still large enough to contain a large number of different frames. For a 12.8% Strehl ratio, the gain in telescope time is still 2.6 and 1.9 for a 10.8% Strehl ratio.

We show in Figure 6 a visual comparison, based on the same dataset, between a classic lucky imaging image for a 1% selection and a 9% selection for ISFAS algorithm, presenting very similar Strehl-ratio performances. A long exposure at the output of the AO has been also added for reference. For this particular figure, photon noise corresponding to a magnitude 12 star in an exposure of 29 milliseconds has been added to the set of frames before analysis. A hexagonal pattern of PSFs of decreasing magnitude has been added in order to show the detection level for each algorithm. This pattern is repeated at different distances

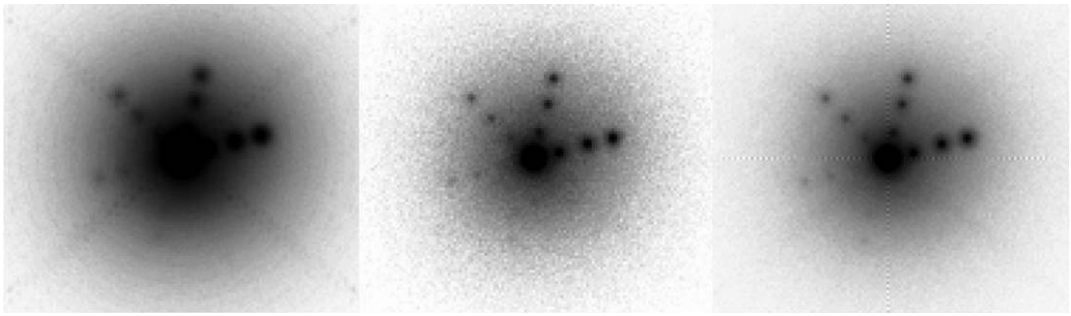

FIG. 6.—Simulated results from two algorithms and an AO-corrected long exposure. The central PSF is a simulated twelfth magnitude star with fainter companions around it in a hexagonal pattern. The magnitude increases from one magnitude between each angular position counter clockwise, starting from $\Delta m = 3$ (inclination $= 15°$ from horizontal, to the right of the star) to $\Delta m = 8$ (inclination $= -45°$) with 30° increment. The images present the same magnitude radially, at 10 pixels, 20 pixels, and 30 pixels from the central star, equivalent to 84, 168, and 252 mas at 650 nm. The dataset is described in previous figures. *Left:* The long exposure time with AO only, equivalent to 9000 images. *Middle:* The classic lucky imaging with a 1% selection, 90 selected images. *Right:* The ISFAS with a 9%, 810 results selected in the Fourier domain for each spatial frequency. Classic lucky imaging and ISFAS have a very similar Strehl ratio performance. Photon noise has been taken into account during this particular simulation using a Gaussian kernel of size 5 pixels and FWHM 2 pixels.

from the central star but still inside the visible halo in order to exhibit the radial influence on the detection level. In this case, the ISFAS technique allows clearer detection of $\Delta m = 7$ fainter stars at 168 and 252 mas from the center star, due to the gain in sensitivity compared to classic lucky imaging.

5. DISCUSSION AND CONCLUSION

We proposed a new lucky imaging algorithm based on the selection of the highest values of the Fourier transform amplitude for short-exposure frames. It demonstrates improved resolution at equal selection compared to a more classic lucky imaging algorithm based on the instaneous Strehl ratio. It mainly benefits the user by strongly increasing the sensitivity of the resultant image or decreasing the total exposure time needed for a given signal-to-noise ratio up to eight times to obtain a 15% Strehl ratio on an AO-equipped 8 m telescope. We also proposed in this article a simple way to reduce photon noise effects on the selection process. The algorithm requires, for now, a low—Strehl-ratio PSF with a "core" to recenter each frame accurately.

The algorithm we present is a simple yet effective approach to resolve a broader problem: how to obtain the best resolution and photometric sensitivity trade-off based on the selection strategy of short-exposure frames in the low—Strehl-ratio regime. Several aspects of this first algorithm can be improved. This algorithm is based solely on the amplitude values of each image, while an algorithm taking into account both amplitude and phase would increase general resolution and sensitivity performances. Finally, on a more profound aspect of the selection itself, this first algorithm is based on the same selection ratio for each spatial frequency: designing an algorithm calibrating a selection ratio based on the signal-to-noise ratio for each spatial frequency would further optimize the lucky imaging approach.

REFERENCES

Babcock, H. W. 1953, PASP, 65, 229
Beckers, J. M. 1983, Lowell Obs, Bull., 9, 165
Cagigal, M. P., & Canales, V. F. 1998, Opt. Lett., 23, 1072
Christou, J. C. 1991, PASP, 103, 1040
Fried, D. L. 1966, J. Opt. Soc. Am., 56, 1372
———. 1978, J. Opt. Soc. Am, 68, 1651
Fusco, T., & Conan, J. 2004, J. Opt. Soc. Am. A, 21, 1277
Garrel, V., Guyon, O., Baudoz, P., Martinache, F., Vogt, F., Takashi, Y., Kaito, Y., & Cantalloube, F. 2010, Proc. SPIE, 7736, 77360N
Gladysz, S., Christou, J., Law, N., Dekany, R., Redfern, M., & Mackay, C. 2008, Proc. SPIE, 7015, 70152H
Gladysz, S., Christou, J. C., & Redfern, M. 2006, Proc. SPIE, 6272, 62720J
Goodman, J. 1996, Introduction to Fourier Optics (2nd ed.; New York: McGraw-Hill)
Guyon, O., et al. 2004, Proc. SPIE, 5490, 733
Hardy, J. W., Lefebvre, J. E., & Koliopoulos, C. L. 1977, J. Op. Soc. Am., 67, 360
Hormuth, F., Brandner, W., Hippler, S., Janson, M., & Henning, T. 2007, A&A, 463, 707
Keremedjiev, M., & Eikenberry, S. S. 2011, PASP, 123, 213
Knox, K. T., & Thompson, B. J. 1974, ApJ, 193, L 45
Labadie, L., et al. 2010, Proc. SPIE, 7735, 77350X
Labeyrie, A. 1970, A&A, 6, 85
Law, N. M., Mackay, C. D., & Baldwin, J. E. 2006, A&A, 446, 739
Law, N. M., et al. 2009, ApJ, 692, 924
Mackay, C. D., Baldwin, J., Law, N., & Warner, P. 2004, Proc. SPIE, 5492, 128
Muller, R. A., & Buffington, A. 1974, J. Op. Soc. Am., 64, 1200
Paxman, R. G., & Seldin, J. H. 1993, Proc. SPIE, 2029, 287
Rodríguez Ramos, L. F., Piqueras Meseguer, J. J., Martin Hernando, Y., Oscoz, A., & Rebolo, R. 2008, Proc. SPIE, 7014, 701449
Roggemann, M. C., & Welsh, B. 1995, Imaging Through Turbulence (Boca Raton: CRC Press)
Rousset, G., Fontanella, J. C., Kern, P., Gigan, P., & Rigaut, F. 1990, A&A, 230, L 29
Weigelt, G. P. 1977, Opt. Commun., 21, 55